Curvature of interatomic surfaces. II. Origin and systematics

A. Martín Pendás[a] and V. Luaña
Departamento de Química Física y Analítica, Facultad de Química, Universidad de Oviedo, E-33006-Oviedo, Spain

(Received 15 May 2003; accepted 21 July 2003)

We investigate the origin of the local curvatures of the interatomic surfaces of the theory of atoms in molecules. The analytic expressions obtained in a previous work are used as a basic guide to this end, and several simplified models of the electron density between a pair of interacting atoms demonstrate that the stiffness difference in the atomic densities near the bond critical points controls their signs and magnitudes. Some steps toward a systematic evaluation of the curvatures of simple molecules have also been taken, and a number of correlations between these curvatures and chemically relevant atomic properties are presented. © *2003 American Institute of Physics.*
[DOI: 10.1063/1.1607964]

I. INTRODUCTION

In a preceding paper,[1] we have presented a systematic study of the geometry of the interatomic surfaces (IASs) of the theory of atoms in molecules (AIM) of R. Bader and coworkers.[2] Previous works regarding this issue[3] had focused on the integration of the Gaussian curvature (K) over the surfaces and on the correlation of this scalar, the integral curvature of an interatomic face (C^F), with different chemically relevant magnitudes. We took a different point of view, and both global and local geometrical properties of the IASs were investigated. The results of this preceding paper, paper I in the following, showed unequivocally that C^F's are not computationally accessible when the IASs are not bounded, and that they are constrained by the global Gauss-Bonnet theorem[4] when they are bounded.

These problems have led us to propose the use of the local value of K at a bond critical point (bcp) K_{bcp} as an standardized measure of the curvature of IASs. We have also shown in Paper I how the principal curvature vectors of the gradient lines of the electron density, ρ, admit analytical expressions at critical points. Using them we have also derived closed formulas for the Gaussian and mean curvatures of IASs at bcp's. As we discussed in Paper I, all these expressions need at most third derivatives of ρ and can be easily coded into any of the standard packages that analyze the topology of the electron density according to the AIM theory.

The first aim of this second paper is to throw light on the origin of the curvatures of IASs. After all, these are salient geometrical features of the atomic images emerging from the AIM theory. Their fundamental origin, however, has never been rationalized satisfactorily. The availability of analytical expressions for K_{bcp} has become essential to attack this problem. We have used a hierarchy of models of ρ, including the promolecular and exponential tail models,[5,6] to construct approximate curvatures that may then be related to known properties of the original models. We will show that it is the stiffness difference in the atomic densities contributing to the density near bcp's which determines K_{bcp}. Since that difference is related to the atomic hardness mismatch between the bonded atoms, the curvatures of IASs correlate with the chemical concept of hardness. This will be used to explain an old puzzle within the AIM theory. It has been noticed repeteadly that, whenever two atoms bond with a significant charge transfer, the atom carrying a negative topological charge lies in the concave part of the IAS. As will become clear, a large part of the geometrical behavior of IASs is, once again, written in the shell structure of the atoms bonded.

The second objective of the paper is to start a systematic study of the variation of K_{bcp} across sets of molecules. Together with the insights obtained from the model curvatures, we expect to uncover interesting correlations between K_{bcp} and a number of chemical concepts. As a by-product, we will discuss the interesting example posed by the B_2H_6 molecule, the first example we have found of a molecule containing a bond with negative Gaussian curvature at the bcp.

The paper is structured as follows. In Sec. II we will study the origin of the curvatures of IASs through the introduction of three models of the electron density in diatomics: the promolecular, exponential, and potential models. Section III will be devoted to discuss the results of Sec. II through the detailed study of a prototypical molecule LiH. Section IV will turn to the systematics of K_{bcp} in a small series of molecules. Finally, Sec. V will summarize our results.

II. ORIGIN OF THE CURVATURE OF INTERATOMIC SURFACES

As previously comented, the curvature of a given IAS near the bond critical point is one of its most easily noticeable geometrical features. However, the lack of local descriptions for separatrices in dynamical systems has made difficult any investigation about its origin. The analytical expressions found in paper I change this scenario, for now it becomes possible to examine the curvatures at bcp's in terms of local derivatives of ρ. Since a large body of knowledge

[a]Electronic mail: angel@fluor.quimica.uniovi.es

regarding the meaning of these derivatives has accumulated over the years, a physically sound interpretation of the origin of curvatures is now at hand.

Let us briefly recall a few concepts from Paper I that will be needed in the following. All the expressions in this paper are referred to the principal reference frame at the critical point. This is the frame formed by the eigenvectors of the Hessian of ρ at the bcp, in such a way that the z axis corresponds to the bond path direction (eigenvector of the positive Hessian eigenvalue at the bcp), and the x,y axes to the orthogonal eigenvectors chosen so as to form a right-handed frame. Let us define the coefficients

$$A_{\alpha\beta\gamma}=\frac{\rho_{\alpha\beta\gamma}}{\rho_{\alpha\alpha}+\rho_{\beta\beta}-\rho_{\gamma\gamma}}, \tag{1}$$

where ρ_α, $\rho_{\alpha\beta}$, and $\rho_{\alpha\beta\gamma}$ are first, second, and third derivatives of the density at the bcp calculated in the principal frame. It follows, then, that the principal normal vectors of the gradient lines along the x,y,z directions at the critical point are

$$\begin{aligned}(\kappa\boldsymbol{n})^x&=A_{xxy}\boldsymbol{j}+A_{xxz}\boldsymbol{k},\\(\kappa\boldsymbol{n})^y&=A_{yyx}\boldsymbol{i}+A_{yyz}\boldsymbol{k},\\(\kappa\boldsymbol{n})^z&=A_{zzx}\boldsymbol{i}+A_{zzy}\boldsymbol{j},\end{aligned} \tag{2}$$

where κ is the curvature of the specified gradient line and $\boldsymbol{n}$ its unit principal normal vector. This is Eq. (18) from paper I written in full detail. Moreover, the Gaussian (K) and mean curvatures (H) at the bcp are

$$\begin{aligned}K&=A_{xxz}A_{yyz}-A_{xyz}^2,\\H&=A_{xxz}+A_{yyz}.\end{aligned} \tag{3}$$

One of the more important advantages of these formulas is the possibility of simplifying the analysis by using approximate analytical models for the electron density around the critical points. We have successfully used this kind of approach to rationalize a number of problems,[5–7] ranging from the values of ionic radii to the existence of non-nuclear maxima of the electron density. As is becoming increasingly clear, many of the topological features displayed by the molecular electron density are controlled by the shell structure of atoms. The curvatures are no exception.

We are going to examine briefly three such models: the promolecular, exponential, and potential models. Each of them will inform us about different aspects of the same problem. We will only consider diatomic molecules. It is clear from Paper I that they contain all of the essential features we want to understand.

Let us then place a diatomic molecule with nuclei A,B located along the z axis at positions $\boldsymbol{r}_a,\boldsymbol{r}_b$. The curvatures $\kappa_x=\kappa_y=\kappa$ are given by the $A_{xxz}=A_{yyz}$ parameters of Eq. (2) At a bcp, $\rho_{xx}<0$ and $\rho_{zz}>0$, so the denominator of A is necessarily negative, and the sign (direction) of the principal curvature vector is determined by ρ_{xxz}.

A. Promolecular model

In the promolecular model, the atomic densities are supposed not to rearrange upon the formation of a molecular state, and the electron density of the diatomic molecule is then given by $\rho=\rho_a(r_a)+\rho_b(r_b)$, where $r_a=|\boldsymbol{r}-\boldsymbol{r}_a|$, $r_b=|\boldsymbol{r}-\boldsymbol{r}_b|$. As a matter of fact, density redistributions are actually very small with respect to the total electron density in all but the lightest molecules. In this approximation, all the needed density derivatives are straightforwardly obtained. The condition of bcp along the z axis is just that of the annihilation of ρ_z and, assuming that the critical point is found between the nuclei, we arrive at $\rho_a'(\text{bcp})=\rho_b'(\text{bcp})=\rho'$. Using this constraint, it is easy to derive the following expression:

$$\kappa_{\text{pro}}=\frac{(\rho_a''/r_a-\rho_b''/r_b)-\rho'(r_a^{-2}-r_b^{-2})}{2\rho'(r_a^{-1}+r_b^{-1})-(\rho_a''+\rho_b'')}, \tag{4}$$

where all derivatives are obtained at the bcp.

As we can see, the promolecular curvature does not involve third derivatives of the atomic densities. This is an important insight, since as far as the promolecular model is a valid approximation, the curvature of the IAS is only determined by the slope and curvature of the atomic densities.

We have obtained the variation of the promolecular curvatures of a series of diatomics with the internuclear distance, R. The atomic densities have been taken from the near Hartree-Fock, multi-ζ exponential wave functions of Clementi and Roetti.[8] As a general rule, the values of κ display a clear shell structure, changing sign (the normal direction) as the different atomic shells penetrate each other. A comparison with *ab initio* curvatures shows that the promolecular model is able to catch the most important features of the behavior of actual molecules, including the repetitive sign change, and that in many cases the agreements are quantitative.

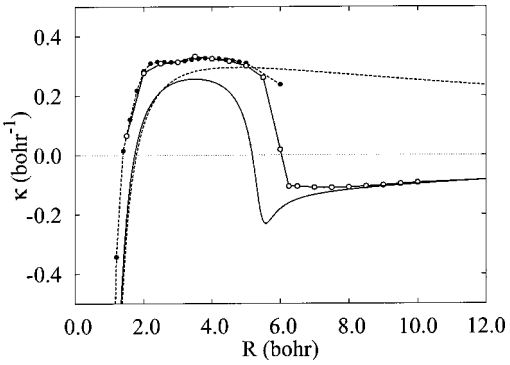

FIG. 1. Evolution of the curvature κ of the IAS of the LiH molecule with the internuclear distance R. The solid line with open circles and the dashed line with solid circles correspond, respectively, to a CAS[4,4]/6-311++G($3dp$,$3df$) and a CISD/6-311++G($3dp$,$3df$) calculations. The solid and dashed lines to the promolecular model from neutral (Li,H) and fully ionized (Li^+, H^-) Clementi–Roetti atomic densities. Curves ending sharply signal convergence problems, as discussed in the text.

Figure 1 shows this kind of comparison for LiH. We have chosen this molecule as an example since it belongs to a rather interesting class of systems with a clear change of adiabatic electronic surface. We have computed the promolecular curvatures for both the ionic state Li^+-H^-, characteristic of configurations close to equilibrium, and the neutral Li–H dissociating limit. The simplest *ab initio* wave function that is expected to behave appropriately in the full distance

range is a complete active space calculation (CAS). We have thus calculated the curvatures at a CAS[4,4]/6-311++G($3dp$,$3df$) level, which has shown convergence problems at short R's, and also at a CISD/6-311++G($3dp$,$3df$) level, which is very similar to the CAS calculation in the equilibrium regime and does not have convergence problems at small distances, but does display them at large R's. Several interesting facts deserve comment. First, it is seen that the neutral promolecular κ's mimic rather well the overall molecular curvatures, even in the clearly ionic regions, where the ionic curve almost overlaps the neutral one. It is known that the promolecular densities coming from ionic or neutral states in simple ionic regimes are indeed very similar. Second, we can observe two sign changes in the curvature. At large internuclear separations, the lithium IAS is concave. On changing to the ionic state it becomes convex, with an appreciable curvature. Finally, it turns concave again. This oscillating behavior is also characteristic of many other scalars, including the Laplacian, and indicates the outstanding role played by the atomic shell structure in establishing many molecular properties. Though the conduct of LiH does not exhaust all the kinds of behavior we have found, we think it exemplifies well our ideas, so we will not extend this subsection any further.

B. Exponential tail model

As previously commented, there is one well-known, but never explained qualitative correlation between the curvature of IASs and the topological charge transfer. Wherever one looks at, convex atomic basins have positive topological charge and *vice versa*. In other words, cations seem to be convex and anions concave.

The exponential model goes a step beyond the promolecular approximation in the simplification of molecular densities. It relies on recognizing[5] that the electron density around bonding regions is very well approximated by a sum of two exponential contributions centered at the nuclei bonded. We write, then, $\rho_a = N_a e^{-\alpha r_a}$ and $\rho_b = N_b e^{-\beta r_b}$. As we have shown,[5] the N_a, N_b, α, and β parameters may be obtained by numerically fitting experimental or theoretical data and are clearly related to the hardness of the atomic densities involved.

Substituting these expressions into Eq. (4) we get

$$\kappa_{\exp} = \left. \frac{(\beta/r_b - \alpha/r_a) + (r_b^{-2} - r_a^{-2})}{2(r_a^{-1} + r_b^{-1}) + (\alpha + \beta)} \right|_{\text{bcp}}. \tag{5}$$

In all the cases we have explored so far,[5,6,9] the N_a, N_b parameters are about a couple of tens of atomic units and the α, β values cluster around a few atomic units. It is also found that if $\alpha > \beta$—that is, if the A density falls more abruptly than that of B—then $r_a < r_b$. This is an easy to understand behavior exemplified by cations, with small, quickly falling densities, and anions, with large, slowly decreasing ρ's. In such a situation, with $\alpha > \beta$ and $r_a < r_b$, it is obvious that Eq. (5) predicts the A center to be convex. Moreover, as it is also very likely that the most diffuse primitive is centered on the B nucleus, the asymptotic form of the surface will radiate from the B center. This is the usual structure of IASs that is found in ionic bonds. Taking into account our previously reported expressions from Ref. 5,

$$r_a^{\text{bcp}} = \frac{1}{\alpha+\beta}\left[\ln\left(\frac{N_a\alpha}{N_b\beta}\right) + \beta R\right],$$

$$r_b^{\text{bcp}} = \frac{1}{\alpha+\beta}\left[\ln\left(\frac{N_b\beta}{N_a\alpha}\right) + \alpha R\right], \tag{6}$$

we can show that in the large-R regime,

$$\kappa_{\exp} \sim \frac{(\beta-\alpha)}{2 + \left(\frac{\alpha\beta}{\alpha+\beta}\right)R}. \tag{7}$$

This is the long-range tail of Fig. 1. Although curvatures tend to zero in the infinite-separation limit, they do so in a rather slow way. Two unequal atoms may then show relatively important curvatures even when at large distances one from the other.

We can conclude that the rationale behind the charge-curvature correlation seems to be found more in the decaying features of the densities of positively and negatively charged species than in a direct cause–effect relationship. In other words, the concave side of the IAS will correspond to the atom carrying the most diffuse function, which is going to be, ususally, the more electronegative one. Actually, these ideas have guided us in finding specific situations in which the correlation is violated. We will find some examples below.

C. Potential model

As a last model, we have found it very instructive to inspect an analytical representation of the electron density around a bcp which contains the minimal elements that allow for nonzero curvatures in IASs. In a certain sense, understanding the sign of the curvature is one of our most interesting goals and, as shown in Eq. (2) this sign is solely determined by the third derivatives of ρ.

The simplest Taylor expansion satisfying these requisites for a diatomic is, referred to our principal reference frame,

$$\rho \sim \frac{1}{2}[\rho_{\parallel}'' z^2 + \rho_{\perp}''(x^2+y^2) + \delta(x^2+y^2)z]. \tag{8}$$

The sign of the κ is here the sign of δ which, in turn, measures how the second derivative of the density along the perpendicular (to the internuclear axis) direction varies on moving onto that axis. Figure 2 is a height representation of the density of such a model in the z-x plane. The IAS curves towards the atom that has a steepest decrease of ρ in the perpendicular direction—i.e., the atom with the stiffest density. It is not necessary that $\rho_{\parallel}$ be asymmetric around the bcp for the IAS to curve; Eq. (8) is always quadratic along z. However, $\rho_{\parallel}''$ and $\rho_{\perp}''$ are not completely independent variables, for they result from appropriately redistributed spherically decaying atomic densities, and it is safe to assume that a stiffer $\rho_{\perp}''$ is also accompanied by a similarly stiffer $\rho_{\parallel}''$.

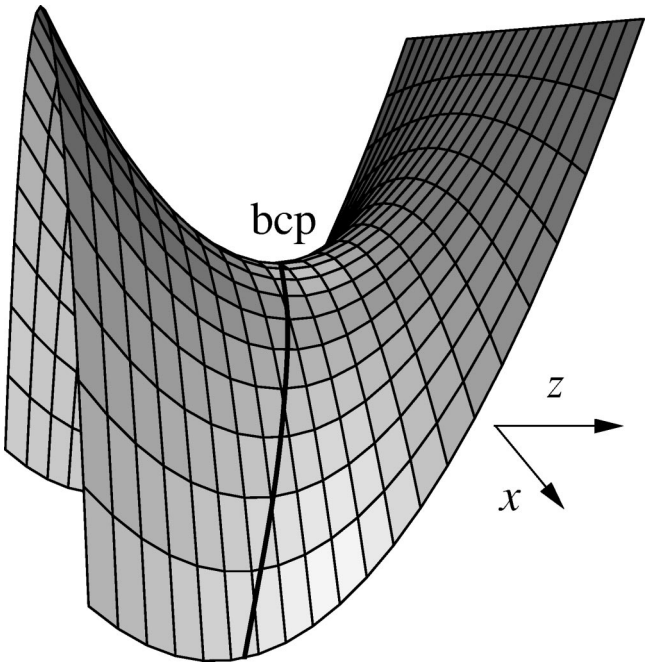

FIG. 2. Bidimensional model surface $\rho = z^2 - x^2 + x^2 z$. The bcp and the gradient line defining the IAS are explicitly shown.

III. DISCUSSION

The tools and insights developed so far may be taken jointly to gain a general image of the processes working to construct the geometry of simple IASs. In this section we will examine them in the LiH diatomic. As we have seen in Fig. 1, the curvature of the LiH IAS changes sign twice with internuclear distance R. Figure 3 displays planar sections of these IASs at selected R's, together with the isolines of $\nabla^2\rho$. The density Laplacian is an indicator of the regions of accumulation (negative values) or depletion (positive values) of density. In our context, it helps us give a physical interpretation of the curvature changes. All the plots have been made using our CAS[4,4] wave functions, except the one at $R = 0.7$ bohr, which comes from the CISD calculation.

At $R = 10$ bohr, both atoms are basically spherical, and the Laplacian beautifully displays the K and L shells of the lithium atom. As Fig. 1 shows, we have just two noninteracting spherical densities. Nevertheless, as we advanced earlier, the curvature of the IAS is far from negligible, with a convex hydrogen. The tail model shows us that the $2s$ electron of the lithium atom is much softer than the $1s$ electron of the hydrogen. In summary, the lithium is large and soft, and the IAS curves towards the hydrogen. At $R = 7.0$ bohr, most of the L shell of Li has suffered a strong polarization process towards the hydrogen. We still are on the neutral electronic surface, but there are clear atomic interactions. The relative size of lithium with respect to hydrogen is decreasing, but the curvature is more or less unaffected. At $R = 5.5$ bohr, we have already jumped over the ionic electronic surface. As seen by the position of the IAS, the H atom has captured the L shell of Li, which is still quite labile. This means that as the lithium's soft density moves towards the hydrogen, the curvature changes sign. As the capture process continues, the curvature increases slightly. Notice how the change of scale slightly deceives the eye. At $R = 3.0$ bohr, very near the theoretical equilibrium distance, we have a typically polarized hydride ion and a spherical Li^+ core with no remnant of a valence shell. This is the situation that is generally found in actual systems where the cations are quite generally convex. As R keeps on decreasing, the hydride core deforms progressively, acquiring a considerable back polarization, while the Li^+ core starts noticing the near-

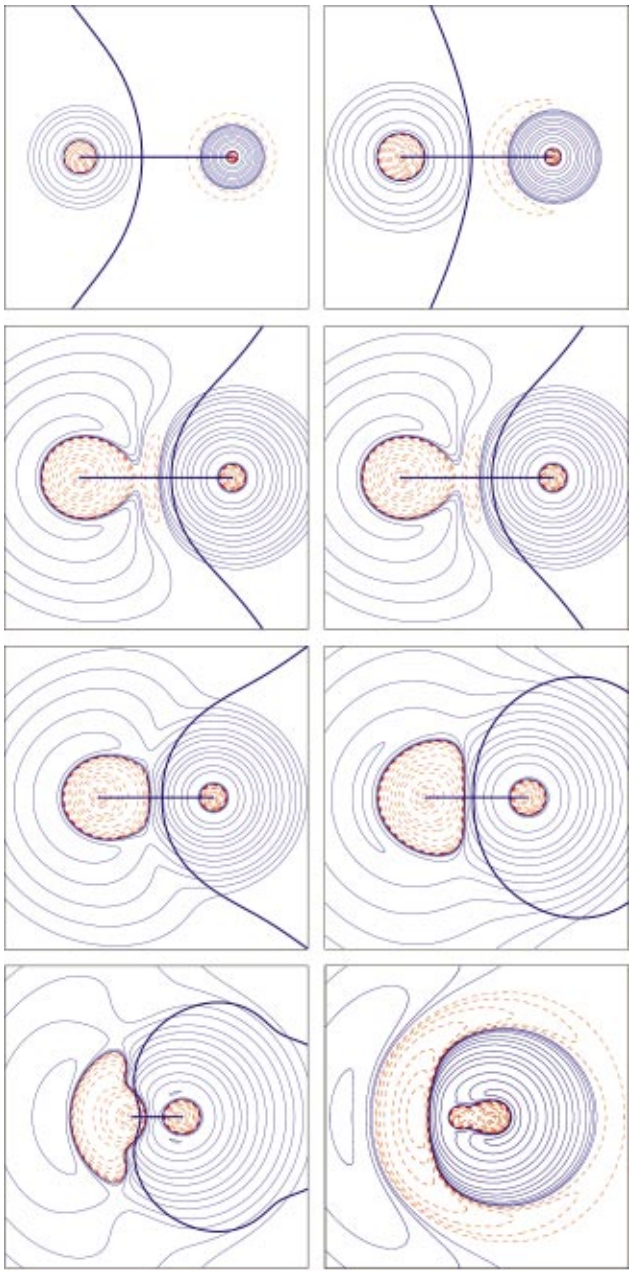

FIG. 3. (color) Projected IASs of LiH in a plane containing the nuclei at selected internuclear distances R. The Li atom is always the rightmost nucleus. Isolines of $\nabla^2\rho$ are also superimposed in a logarithmic scale containing 20 lines that span the range $10^{-3} < |\nabla^2\rho| < 10^3$ a.u. Solid and dashed isolines correspond to positive and negative Laplacians, respectively. The internuclear distances are, from left to right, top to bottom: 10.0, 7.0, 5.5, 4.0, 3.0, 2.0, 1.0, and 0.7 bohr. No bcp is found at $R = 0.7$ bohr. The κ values at the bcp are, in the same order, -0.0925, -0.1088, 0.2608, 0.3243, 0.3130, 0.2760, and -1.5706 bohr^{-1}. Notice that the scales are not the same, so it is difficult to compare the curvatures by simple visual inspection. More computational details are found in the text.

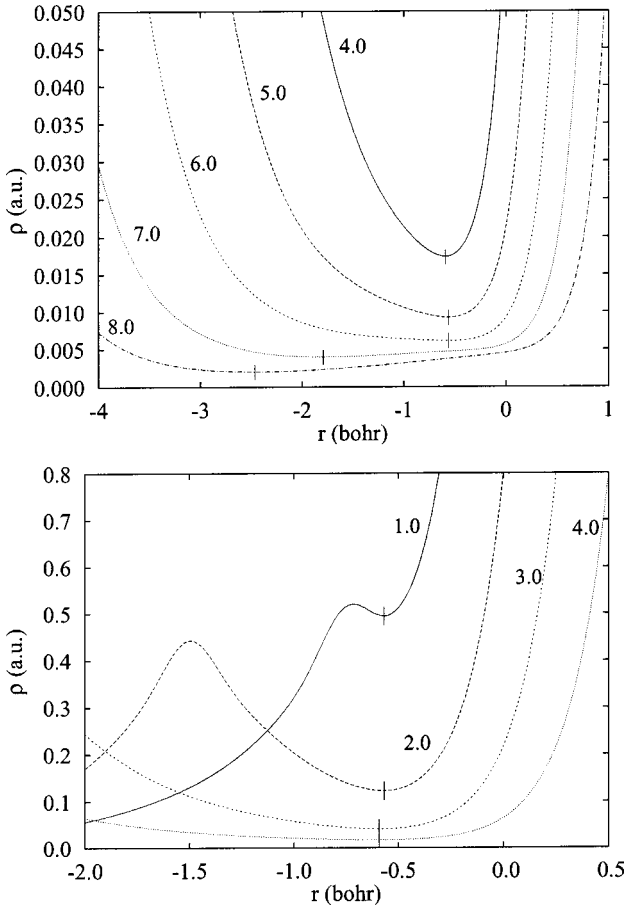

FIG. 4. Density of LiH along the molecular axis in the region around the bcp. Different curves correspond to different internuclear distances. The lithium atom is always located rightmost, and the center of mass of the diatomic is conserved. The bcp position is marked by a small dash for each curve. Top: long-distance regime $R=8.0$, 7.0, 6.0, 5.0, 4.0 bohr. Bottom: short-distance regime $R=4.0$, 3.0, 2.0, 1.0 bohr. All data in atomic units. See the text for computational details.

ness of the hydride. At $R=1.0$ bohr, we can see very neatly these effects. The interatomic surface has penetrated the H^- core, and κ changes sign again. Finally, at $R=0.7$ bohr, a portion of the cores fuse, forming a pseudonucleus with only one maximum of the electron density, the interatomic surface disappears, and a kind of new L shell develops around the new center. We are approaching the united atoms limit. We must, however, be cautious in this regime, for Gaussian basis sets are unable to simulate the nuclear cusps, and the latter will surely play a role in determining the precise point where one of them disappears.

We think that the previous discussion, together with Fig. 1, illuminates the physical meaning of all our previous arguments. Let us finally present the evolution of the density along the molecular axis with R. This kind of study has been done in great detail within the AIM theory by Hernández-Trujillo and Bader,[10] who have followed the topological aspects of the formation of bonds in diatomics. They did not discuss in detail, however, the variation of the curvatures of IASs in the process. Figure 4 gathers this information in two regimes. At large R, onto the neutral electronic surface, the bcp is nearer the H atom. We can perfectly distinguish the L shell bump corresponding to a neutral Li, and in Fig. 3 the lithium conserves its valence shell. It is worth noticing that a logarithmic plot of the lithium's density shows two linear segments corresponding to two decaying scales: the one associated with the K core and that related to the valence shell. If we concentrate on the region near the bcp, we see that the H atom side is stiffer than that of Li. In terms of the exponential model, the hard exponential is associated with the hydrogen and the separatrix curves towards it. However, if we obtain the topological charges of the atoms in this zone, we get, for instance, $Q_{\mathrm{Li}}=+8.60\times10^{-3}|e|$ at $R=10.0$ bohr and $+0.158$ a.u. at $R=7.0$ bohr. The softer density contributes to increase the H electronic charge. This is a general result, and many other systems with IASs violating the alleged charge-curvature correlation have been found, almost always at nuclear configurations far from equilibrium.

It is very satisfying that the Born-Oppenheimer avoided crossing related to the jump from the neutral to the ionic state coincides with a well-defined cusp catastrophe in the density. On going from $R=7.0$ to 6.0 bohr, the point of inflection fuses with the bcp. In the new situation, the bcp is now closer to the Li. Accompanying this catastrophe, κ changes sign, as seen in Fig 3, and the lithium's L shell is absorbed by the hydrogen. The absorption changes the lateral asymmetry of ρ around the bcp, and the situation corresponds now to that of a very hard lithium core and a rather soft hydride. We can pinpoint very precisely when this transition takes place, which we may identify with the ionization process. As a matter of fact, the Li topological charge increases abruptly, changing from $Q_{\mathrm{Li}}=+0.16|e|$ at $R=7.0$ bohr to $Q_{\mathrm{Li}}=+0.70|e|$ at $R=6.0$ bohr and $Q_{\mathrm{Li}}=+0.78|e|$ at $R=5.0$ bohr. We have also found this cusp mechanism in the interesting polarity inversions of low heteropolarity semiconductor crystals.[11]

The ionic picture has a wide range of stability in LiH. Notice how the position of the bcp, relative to the center of mass, is almost independent of the internuclear distance in this regime. This indicates two well-defined exponentially decaying shells in interaction. On decreasing R, the Li topological charge increases, although slightly: at $R=3.0$ bohr it is $+0.885|e|$. Finally, at around $R=1.9$ bohr, the curvature starts to decrease as the cores interact. At $R=1.0$ bohr, the bcp has crossed the zero Laplacian isosurface. It is so near the H maximum that the perpendicular second derivatives counteract the effect of $\rho_{\|}''$. This effect is more important in the direction pointing towards the H atom, this being the condition discussed in our potential model for the IAS to curve in that direction. The proximity of the H nucleus makes the density stiffer along the hydrogen. The sign of κ becomes negative, and some of the density previously associated with the hydride returns to the lithium. At $R=1.0$ bohr, $Q_{\mathrm{Li}}\sim0.8|e|$.

In summary, it is possible to rationalize the origin of the curvature of IASs in terms of physically sound ideas. Though we have only discussed in detail diatomic molecules, our arguments are general. In most cases, only the two atoms bonded contribute appreciably to their IAS near the bcp, so everything applies literally. In some particular situations, a

TABLE I. Some properties at the bcp for some hydrogen-saturated compounds of the second period. HF/TZV++$(2p,3df)$ calculations at the theoretical equilibrium internuclear distances R. All data in atomic units.

System	R	K	$\nabla^2\rho$	ρ	Q_H
LiH	3.0303	−0.1005	+0.1420	0.0390	−0.9040
BeH_2	2.5152	−0.2427	+0.2225	0.0971	−0.8511
BH_3	2.2434	−0.1780	−0.3180	0.1862	−0.6960
CH_4	2.0446	+0.1019	−1.0436	0.2837	−0.0354
NH_3	1.8868	+0.3510	−1.9089	0.3552	+0.3550
H_2O	1.7766	+1.5433	−3.0992	0.3883	+0.6322
HF	1.6956	+3.5514	−3.8718	0.3945	+0.7765
C_2H_2	1.9533	+0.16408	−1.2479	0.3022	+0.1609
C_2H_4	2.0347	+0.11819	−1.0821	0.2905	−0.0611
C_2H_6	2.0484	+0.09541	−1.0419	0.2838	−0.0502

third or, at most, a few more atoms do have some influence, and their role may be introduced along our same lines of reasoning.

IV. LOCAL CURVATURE OF IASs AS A MOLECULAR PROPERTY

In this section we are going to profit from the expressions and ideas presented so far to study the variation of the local curvatures of IASs at bcp's for collections of molecules at their equilibrium nuclear configurations. The values obtained will be correlated with other meaningful magnitudes, and in doing so, some new interesting ideas will pop up. We do not intend to be exhaustive, so just a few representative values will be actually presented. No effort has been made to obtain high-quality theoretical wave functions, since our local curvatures, like other local molecular properties at bcp's, do not depend critically on very-well-balanced basis sets, correlation effects, or other computational parameters that are relevant in the computation of the energy. Most results will refer to Hartree–Fock calculations with reasonable basis sets.

Let us first consider the hydrogen saturated molecules of the second period. Table I gathers a few of the scalars calculated at the bcp, including the Gaussian curvature K, together with the topologically determined net charge of the H atom. First, we observe that the usually called hydrides LiH, BeH_2, and BH_3 display IASs curving towards the nonhydrogen atom, with topological charges consistent with their nominal oxidation states. The largest curvature for this group of three is found in BeH_2. CH_4 is an interesting system, as it marks the sign change for the curvatures in the series, constituting one additional example of curvatures violating the charge-curvature correlation, though the negative charge of the H atom is very small. On moving towards HF we increase significantly both the charge on hydrogen and the curvature of the IAS towards it. Actually, the HF curvature is one of the largest ones we have ever found.

The previous sequence may be understood, including the local maximum of $|K|$ at BeH_2, as a combination of two factors. On the one hand, both Li and Be have almost lost their valence electrons toward the hydrides. The bcp's are located in a positive Laplacian region, corresponding to a very stiff Li or Be density, and a soft H decay, so the decay exponent should be much larger in the Be core than in the Li one. Moreover, the internuclear distance has decreased, and the curvature in BeH_2 is considerably larger than in LiH. In BH_3, the bcp is inside the negative Laplacian region. As a result, the B atom has not lost all of its valence density, and the charge on hydrogen is smaller. The conservation of part of the valence makes the decay exponent that we can associate with the boron also smaller than the one it would have if the bcp were located at the B core. Instead of increasing in absolute value, $|K|$ decreases. This tendency cannot be stopped, and as the distance of the bcp to H decreases and the density derivatives increase due to smaller internuclear equilibrium distances, K increases abruptly.

It is tempting to relate curvatures to electronegativity (χ) differences. After all, in Table I the sign change occurs in methane, and the $\Delta\chi$ value between carbon and hydrogen is nearly zero, and methane also marks the sign change in $\Delta\chi$. Table II shows the curvatures of the hydrides, fluorides, and chlorides of Li and Na. We have changed the basis set, 6-311G(p,d) this time, to show how transferable are curvatures with computational conditions in LiH. We can clearly see that there is not a simple correlation between χ and κ. This has already been put forward by Popelier,[3] who also established the relationship between the integrated curvature and the difference in chemical hardness, or deformability, of the intervening densities. Actually, there are not many chemically sound atomic magnitudes[12] with similar values for hydrogen and fluorine, two atoms that, on the other hand, do not share many chemical properties. The promolecular or exponential models support this view, for the decay rate of the atomic density is directly related to the polarizing or

TABLE II. Curvature at bcp versus electronegativity difference for a few binary compounds at the HF/6-311G(p,d) theoretical equilibrium distances. All data in atomic units, except electonegativities, in a standard Pauling scale.

System	R	K	$\nabla^2\rho$	ρ	$\Delta\chi$
LiH	3.0301	0.10704	0.1621	0.03895	1.22
LiF	2.9462	0.10619	0.7769	0.07332	3.00
LiCl	3.8507	0.15614	0.2598	0.04281	2.18
NaH	3.6186	0.02132	0.1287	0.03109	1.27
NaF	3.6141	0.01847	0.4829	0.05321	3.07
NaCl	4.5295	0.04647	0.1864	0.03160	2.23

deforming ability of the species, which is usually controlled by its ionization potential.

The formation of the curvature of an IAS, from this point of view, may be seen as a competition to distort the spherically decaying atomic density of the bond companion. Li^+, a very polarizing agent indeed, distorts more easily the density of chlorine than that of fluorine. The softer the atoms involved, the smaller the curvatures. It is nevertheless necessary to take these correlations with care, since there are a number of variables determining κ, like bond distances, which are not taken into account in the usual definition of hardness. For instance, HCl, with a very polarizing proton and a softer base than fluoride, has a K value around 0.33 a.u., much smaller than the curvature of the IAS of HF. We also feel that the relationship between the asymptotic decay of molecular densities and ionization potentials, on the one hand, and between the latter and the concepts of electronegativity and hardness within density functional theory[13] implies a link that deserves further study.

There have been a number of successful attempts to relate electronegativity and hardness with properties at critical points. Particularly interesting in our context are the works by and co-workers.[14] These authors have shown that, using Gasquez and Ortiz's.[15] result that atomic hardness and atomic size are inversely proportional, one can use the ratio of atomic radii at the bcp as the inverse ratio of their relative hardness, η: $\eta_A r_a^{\mathrm{bcp}} = \eta_B r_b^{\mathrm{bcp}}$. If we look at our Eq. (6) and take into account that the logarithmic terms are usually smaller than those proportional to R, we see that the exponential parameters are actually playing the role of the atomic η's and that the κ values are related to $\Delta\eta$. Additional support for these ideas can be found in Table I. It is shown that the curvatures of the C-H IAS in ethane, ethene, and ethyne increase in this order, revealing a decreasing hardness of carbon along the series, as is well established. Notice again how the change in curvature is not directly related to topological charges.

This example does not exhaust the possible correlations between the curvature of IASs and atomic properties. For instance, we have found that the ratio H/ρ, where H is the mean curvature, correlates fairly well with $\Delta\chi$ in the compounds of Table I. We will not pursue these studies any further here, but we will instead turn to consider other features revealed by the curvatures of IASs.

As we have tried to show, the local values of the curvatures of IASs at the bcp carry chemical information about the atoms forming the surface and their chemical environment. We have also discovered that they give us a kind of information about the nature of the bond that is not easy to obtain from other local topological indices. We can bring to light these ideas by analyzing the well-known topology of the diborane molecule. Figure 5 shows the molecular graph of diborane together with the reference frames for its two different B-H bonds, which we have named the terminal, t, and bridge, b, B-H bonds. The planes depicted correspond to the osculating planes of the two different IASs, for they are orthogonal to the direction defined by the eigenvector of the Hessian of ρ along the bond path.

Table III gathers the $\kappa\boldsymbol{n}$ normal vectors along the three

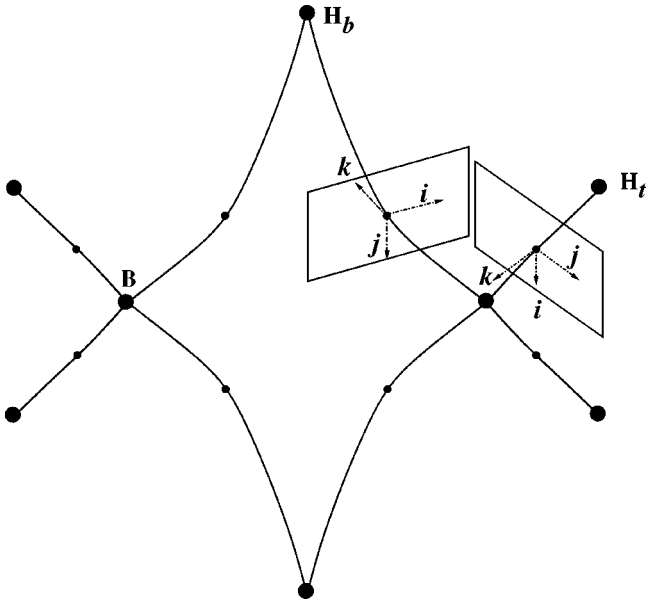

FIG. 5. Schematic diagram showing the principal frames of the two types of B–H bonds (terminal, t, and bridge, b) in the B_2H_6 molecule. We show the molecular graph as calculated at the HF/6-311G(p,d) equilibrium geometry, with nuclei and bond points marked with large and small circles, respectively. The planes onto which the principal frames are located correspond to the osculating planes of the IASs. Notice the large curvature of the bond B–H_b bond path.

eigendirections of the Hessian for the two bcp's. These correspond exactly to the vectors defined in Eq. (2) The terminal B-H bond in the B_2H_4 plane has the following Hessian frame: $\boldsymbol{i}$ is normal to the plane, $\boldsymbol{k}$ points to the boron in the bond direction, and $\boldsymbol{j}$ is orthogonal to $\boldsymbol{k}$ and points towards the B-B axis. The gradient lines that escape this bcp in the x direction curve towards the nearest boron, with a curvature of about 0.30 a.u. They do also curve slightly against its neighboring H_t. We have found that these secondary curvatures seem to be a rather general feature of gradient lines when nonbonded atoms exist in their proximities and symmetry allow for them. The gradient lines escaping along the y direction are pure parabolas in the y-z plane to second order. They also curve towards the neighboring boron, this time with $\kappa \sim 0.17$ bohr^{-1}.

We can compare these values with those of the B-H bond in BH_3. The equivalent numbers are 0.52 and 0.34 a.u., respectively. These are larger due, mostly, to the shortening

TABLE III. Normals, $\kappa\boldsymbol{n}$ of the Hessian eigenvectors at the bcp for the two different B—H bonds in diborane: the B—H bond in the B_2H_4 plane, and the bridging electron deficient B—H bonds. The $\boldsymbol{i}$, $\boldsymbol{j}$, $\boldsymbol{k}$ are, respectively, the x,y,z unit vectors of the Hessian eigenvectors frame. See the text for details. All data refer to a HF/6-311G(p,d) calculation at the theoretical minimum and are presented in atomic units.

B—H bond	$\kappa\boldsymbol{n}$	$\boldsymbol{i}$	$\boldsymbol{j}$	$\boldsymbol{k}$
Terminal	$(\kappa\boldsymbol{n})^x$	0.0000	+0.0351	+0.2959
Terminal	$(\kappa\boldsymbol{n})^y$	0.0000	+0.0000	+0.1659
Terminal	$(\kappa\boldsymbol{n})^z$	0.0000	+0.1297	+0.0000
Bridge	$(\kappa\boldsymbol{n})^x$	0.0000	+0.1586	+0.1323
Bridge	$(\kappa\boldsymbol{n})^y$	0.0000	+0.0000	−0.1237
Bridge	$(\kappa\boldsymbol{n})^z$	0.0000	−0.9701	+0.0000

of the B-H distance on going from diborane to borane. What is interesting in this comparison is that the curvature in the plane of bonds is smaller than that in the orthogonal direction both in BH_3 and B_2H_6. This is easily interpreted in terms of the flattening effect of neighboring atoms in the decay rate of ρ. Finally, the very bond path line has a non-negligible curvature of about 0.13 a.u., bending the B-H_t bonds towards the B-B line. The joint effect of these effects give rise to a small Gaussian curvature for the B-H_t IAS, $K=0.2959\times 0.1659=0.0491$ bohr^{-2}. Though slightly asymmetric about the x and y directions, it is otherwise perfectly a normal surface.

Let us turn to the B-H_b IAS, which is indeed outstanding. In this case, $\boldsymbol{i}$ is normal to the B_2H_2 bridging plane, $\boldsymbol{k}$ points towards the hydrogen in the bond direction, and $\boldsymbol{j}$ is contained in the bridging plane pointing towards the B-B axis. The gradient lines along the x direction curve towards the H_b, with a curvature similar to that found along the y direction in the terminal bond. Notice, however, that the secondary curvature along the y direction, $\sim +0.16$ a.u., is now even larger that the primary curvature. Moreover, the gradient lines along the y direction display a *negative* primary curvature of about -0.12 bohr^{-1}, curving towards the neighboring boron. This means that the IAS has a *negative* Gaussian curvature, $K=-0.1237\times 0.1323=-0.0164$ bohr^{-2}. The IAS is saddle shaped in the vicinity of the bcp. Finally, the curvature of the B-H_b bond path line is extremely large, about half the value of the curvatures of gradient lines in HF, which has the largest values we have found so far.

The curvatures of the gradient lines at the B-H_b bcp seem to signal some of the relevant aspects of this three-center, two-electron bond. We have only found negative K's in deficient electron boranes, but our search has been far from complete. It remains to be seen if this is indeed a property of such bonds, but if this conjecture is confirmed, then a local, simple-to-obtain index might be used as a signature of these interesting kind of bonds.

V. CONCLUSIONS

This work complements the results obtain in the preceding paper[1] regarding the curvatures of the interatomic surfaces of the AIM theory. We have focused here on the origin and variability of the local curvatures at bond critical points.

The availability of the analytical expressions for K derived in paper I has been key to investigate the origin of the curvature of IASs. By using several simple models of the electron density around a bond critical point, we have been able to show that the variation of curvatures with geometric parameters is a consequence of the shell structure of atoms. As found in other situations, the promolecular model is an excellent predictor of the behavior of ρ around bcp's. Simple arguments explain the values and sign of the observed curvatures. As a by-product of our analyses, we have shown that no strict correlation exists between the topological charge and the curvature of IASs. Actually, K is determined by the decay rate of the atomic densities involved in the bond under study. Given the relation between the hardness or softness of a given species and its ability to attract or release electrons, the topological charge of most basins at the equilibrium configuration does correlate with the curvature, though counterexamples have been found far from equilibrium.

The first steps towards a systematic investigation of local K's in actual systems have also been undertaken. We have found that the local curvature is fairly transferable among systems and that the differences found in equivalent bonds are related to changes in the chemical environment surrounding the IAS. The curvature is intimately related to the concept of atomic hardness, and further work along these lines should be done in the future. Finally, some negative curvature surfaces have been found in deficient electron bonds. The generality of this finding does also deserve further exploration.

The expressions that we have found have been coded in our topological programs and are very easily transferred to other codes. We hope that they may be of use in the future.

ACKNOWLEDGMENT

This work has been partially supported by the Spanish Ministerio de Ciencia y Tecnología, Project No. BQU2000-0466.

[1] A. Martín Pendás and V. Luaña, J. Chem. Phys., **119**, 7633 (2003) (preceding paper).
[2] R. F. W. Bader, *Atoms in Molecules* (Oxford University Press, Oxford, 1990).
[3] P. L. A. Popelier, Can. J. Chem. **74**, 829 (1996).
[4] M. P. do Carmo, *Differential Geometry of Curves and Surfaces* (Prentice-Hall, Englewood Cliffs, NJ, 1976).
[5] A. Martín Pendás, A. Costales, and V. Luaña, J. Phys. Chem. B **102**, 6937 (1998).
[6] A. Martín Pendás, M. A. Blanco, A. Costales, P. Mori Sánchez, and V. Luaña, Phys. Rev. Lett. **83**, 1930 (1999).
[7] A. Martín Pendás, V. Luaña, L. Pueyo, E. Francisco, and P. Mori Sánchez, J. Chem. Phys. **117**, 1017 (2002).
[8] E. Clementi and C. Roetti, At. Data Nucl. Data Tables **14**, 177 (1974).
[9] A. Martín Pendás, A. Costales, M. A. Blanco, J. M. Recio, and V. Luaña, Phys. Rev. B **62**, 13970 (2000).
[10] J. Hernández-Trujillo and R. F. W. Bader, J. Phys. Chem. A **104**, 1779 (2000).
[11] P. Mori Sánchez, A. Martín Pendás, and V. Luaña, Phys. Rev. B **63**, 125103 (2001).
[12] R. G. Parr and R. G. Pearson, J. Am. Chem. Soc. **105**, 7512 (1983).
[13] R. G. Parr and W. Yang, *Density-Functional Theory of Atoms and Molecules* (Oxford University Press, New York, 1989).
[14] R. J. Boyd and S. L. Boyd, J. Am. Chem. Soc. **114**, 1652 (1992); L. Komorowski, S. L. Boyd, and R. J. Boyd, J. Phys. Chem. **100**, 3448 (1996).
[15] J. L. Gasquez and R. Ortiz, J. Chem. Phys. **157**, 45 (1991).